Catalysis Today xxx (2016) xxx–xxx

Contents lists available at ScienceDirect

Catalysis Today

journal homepage: www.elsevier.com/locate/cattod

Propane oxidative dehydrogenation over VO_x/SBA-15 catalysts

Gheorghita Mitran[a], Rawaz Ahmed[b,1], Emmanuel Iro[b], Saeed Hajimirzaee[b], Simon Hodgson[b], Adriana Urdă[a,*], Maria Olea[b], Ioan-Cezar Marcu[a,*]

[a] Laboratory of Chemical Technology and Catalysis, Department of Organic Chemistry, Biochemistry and Catalysis, Faculty of Chemistry, University of Bucharest, 4-12, Blv. Regina Elisabeta, 030018 Bucharest, Romania
[b] School of Science and Engineering, Teesside University, Middlesbrough, United Kingdom

ARTICLE INFO

Article history:
Received 15 September 2016
Received in revised form 2 December 2016
Accepted 7 December 2016
Available online xxx

Keywords:
Oxidative dehydrogenation
Propane
Supported vanadia catalysts
VO_x/SBA-15

ABSTRACT

VO_x/SBA-15 catalysts with five different vanadium loadings were prepared by a modified wet impregnation method, characterized using N_2 adsorption, XRD, EDX, SEM, Raman and UV–vis spectroscopies and H_2-TPR techniques, and tested in the oxidative dehydrogenation of propane in the temperature range 450–600 °C. For all the catalysts the propane conversion increases with both reaction temperature and vanadium loading, while the selectivity for propene decreases mainly to the benefit of carbon oxides. Several types of VO_x species coexist on the catalyst surface, with monomeric and low-polymerized ones leading mainly to propene, while V_2O_5 crystallites at high vanadium loadings producing more carbon oxides. Propene was determined to be the only primary product irrespective of the vanadium content.

1. Introduction

The increasing demand in unsaturated hydrocarbons for the manufacturing of polymers, synthetic fibers, detergents, elastomers and synthetic fuels, has triggered the development of inexpensive and environmentally friendly ways of their production. The lower price of alkanes compared to the corresponding alkenes makes their use as feedstock in the chemical and petrochemical industry very attractive [1–3]. However, the current alkanes conversion technology, based on the dehydrogenation process, has several disadvantages, such as high endothermicity, unfavorable equilibrium shift and difficult control of cracking side reactions at high temperatures, which contribute to the rapid coking of the catalyst [1,3,4]. Therefore, the alternative conversion route consisting in the oxidative dehydrogenation (ODH) process becomes promising from engineering and economic points of view by overcoming all these drawbacks [1,5–7]. The main problem remains avoiding side reactions leading to oxygen-containing organic molecules and carbon oxides, which severely limit the selectivity to dehydrogenation products [1,8,9]. Early attempts to use other oxidants (i.e. iodine) were abandoned due to corrosion and environmental problems posed by the oxidant [1]. Recently, N_2O was also used as oxidation agent in ODH reactions with interesting results [10,11].

Many catalysts have been tested for the ODH reaction, but supported vanadia and molybdena proved to be the most active and selective ones [12]. In both cases, the most selective catalysts contain well-dispersed vanadium or molybdenum species onto the support surface, at near monolayer coverage, which is about 7.5 V nm^{-2} for polyvanadate [13] and about 4.8 Mo nm^{-2} for polymolybdate; however, vanadia has higher ODH activity than molybdena at equivalent dispersion [6]. Notably, much lower values corresponding to the monolayer coverage were more recently proposed for catalysts supported on silica (0.7 V nm^{-2}) and explained by the lower density and reactivity of silica surface hydroxyl groups [8]. Vanadium oxide catalysts supported on various oxides, such as SiO_2, Al_2O_3, TiO_2, Nb_2O_5, MgO, La_2O_3, Sm_2O_3 and Bi_2O_3, to mention some of them, have been extensively studied [1,7,14,15]. Their catalytic performance in the ODH of alkanes depends on the nature of the support (which, in turn, is partly responsible for the vanadium reducibility and dispersion), the vanadium loading and the preparation conditions, which influence the nature and structure of the VO_x surface species [5,15]. Moreover, the acid-base character of the support affects the catalytic performance [15]. It has been found that in the ODH of propane the most selective catalysts were obtained with vanadium supported on basic, rather than on acidic metal oxides. It has also been found that VO_x species with V in octahedral and tetrahedral positions are the active ones, the tetrahedral being less active but more selec-

* Corresponding authors.
E-mail addresses: adriana.urda@chimie.unibuc.ro (A. Urdă), ioancezar.marcu@chimie.unibuc.ro (I.-C. Marcu).
[1] Present address: Kurdistan Institution for Strategic Studies and Scientific Research (KISSR), Qirga, Slemani, As Sulaymaniyah, Iraq.

http://dx.doi.org/10.1016/j.cattod.2016.12.014
0920-5861/

tive. The higher the concentration of VO^{2+} and V_2O_5 species the lower is the selectivity to propene [16]. The presence of polymerized vanadium species and bulk V_2O_5 is detrimental to the activity of the catalyst as well, as less vanadium atoms are accessible to the propane molecules. In order to minimize the formation of V_2O_5 crystallites responsible for the formation of CO_x, oxide supports with high surface area and lower reducibility than vanadia are used [6,7,17]. The support plays an important role in the dispersion of the active phase, on the accessibility, reactivity and acidity of the active sites, and also on the mass/heat transfer phenomena [18]. Combining the textural and acid-base properties of the support with the redox properties of the vanadia species makes it easier to activate alkanes at lower temperatures [19].

Silica-supported vanadia catalysts were reported to be active in propane ODH [5] and, in order to increase the propene yields, mesoporous siliceous materials such as MCM-41, MCM-48, mesocellular foams (MCF) and SBA-15 were used as supports [5,20,21]. SBA-15 is a mesoporous silica, characterized by large surface area and formed by a hexagonal array of uniform tubular channels, with tunable pore diameters in the range of 5–30 nm and very narrow pore-size distribution [22,23]. It has been used as support for catalysts in the ODH of butanes [24,25], ethane [26], ethylbenzene [11], as well as for methanol oxidation [23,27].

Propane ODH on vanadia supported on mesoporous SBA-15 has been studied by several groups [17,22]. However, since both silica and vanadia possess acidic character, it is very challenging to prepare catalysts with high dispersion at high loadings. Therefore, the preparation method and conditions should be carefully chosen. Some of the preparation methods used so far are: alcoholic impregnation [20,22], wet impregnation [17,24,28], mechanical mixing [22], direct synthesis [18,29], adsorption [22] and grafting-ion exchange [27,30,31]. Although superior performances of the mesoporous VO_x/SBA-15 catalysts have already been reported [22], a fundamental understanding of their behavior towards the propane ODH remains to be accomplished.

The aim of this paper is to investigate further the catalytic activity of the SBA-15-supported vanadia catalysts and to gain a deeper insight into their structure-activity relationship. In order to accomplish these goals, a series of VO_x/SBA-15 catalysts, with vanadium loadings between 6.5 and 11 wt%, were prepared using an improved impregnation method and their detailed characterization by N_2-adsorption, SEM/EDX, XRD, H_2-TPR, Raman and UV–vis spectroscopies as well as their catalytic performance in the oxidative dehydrogenation of propane have been performed.

2. Experimental

2.1. Support preparation

The general experimental procedure followed in the preparation of SBA-15 mesoporous silica was described in detail by Zhao et al. [32]. However, this procedure was modified and the preparation conditions, such as the amount of P123, type of acid and aging time, were optimized through experiments. The optimized procedure is described below.

4 g of Pluronic 123 triblock copolymer (EO20-PO70-EO20, P123, Sigma-Aldrich) was dissolved into 120 g of deionised (DI) water at 40 °C, under vigorous stirring for 6 h. Then 20 ml of 2 M HCl (Fisher Scientific) was added to the clear solution and after 10 min, 9.25 g of TEOS (Tetraethylorthosilicate, Sigma-Aldrich) was introduced dropwise, the solution being kept under vigorous stirring at 40 °C for 20 h. A white precipitate was formed which was kept in an oil bath at 95 °C for 24 h, without stirring, then filtered, washed with 600 ml of deionised water and dried at 60 °C for 24 h. The white powder was then calcined at 550 °C, under steady-state conditions, for 6 h, at a heating rate of 10 °C min^{-1}. After calcination, the sample was cooled down to 60 °C at a cooling rate of 10 °C min^{-1} and placed in a round bottom flask with a short condenser inside to be re-hydrated by using 50 g of DI water. The suspension was then placed in an oil bath at 105 °C and left boiling under a gentle stirring. After 2 h, the suspension was filtered and 2 g of SBA-15 sample were collected by filtration and dried a 120 °C for 6 h.

2.2. Catalyst preparation

Five SBA-15-supported vanadia samples were prepared by wet impregnation. A solution of ammonium vanadate, NH_4VO_3 (Sigma-Aldrich), was contacted with the SBA-15 support, under stirring, at 55–60 °C for 2 h, to achieve a final V content of 6.5–11.0 wt%. The solid product was recovered by filtering and then dried in vacuum, at 100 °C, for 1 h, followed by calcination in air at 600 °C, for 5 h, at a heating rate of 5 °C min^{-1}. The impregnated samples were labelled as *x*V, where *x* denotes the wt% of V.

2.3. Catalysts characterization

The textural characterization was performed using the nitrogen adsorption/desorption method, with a Micromeritics ASAP 2010 automatic equipment. The surface areas were calculated using the BET method in the relative pressure, P/P_0, region 0.065–0.2, while the pore sizes were determined by the BJH method from the nitrogen desorption branch. Prior to nitrogen adsorption, the samples were degassed at 150 °C for 10 h.

Scanning Electron Microscopy (SEM) accompanied by X-ray energy dispersion analysis (EDX) was used to monitor the morphology and surface composition of the catalysts samples. SEM/EDX examination was performed using a Hitachi S-4500 field emission microscope with a Quartz PCI XOne SSD X-ray analyser.

To obtain information on both, the mesoporous structure and the crystalline structure of the SBA-15-supported vanadia catalysts, small- and wide-angle X-ray diffraction (XRD) patterns were recorded on a Bruker D8 (25 kV, 20 mA) powder X-ray diffractometer, using Cu Kα radiation (λ = 0.15406 nm), a tube voltage of 40 kV, and a current of 20 mA. The data were collected from 0.5 to 4° (2θ) with a resolution step size of 0.01° (small-angle XRD patterns) and from 10 to 70° (2θ) with a resolution step size of 0.02° (conventional wide-angle XRD patterns).

The type of V species formed on the surface of the SBA-15 was studied with Raman spectroscopy. The Raman spectra were recorded with a Raman Microscope Spectrometer Horiba Jobin Yvon – Labram HR UV–vis-NIR, between 100 and 1200 cm^{-1}, using a 633 nm wavelength for excitation. Before recording the spectra, the spectrometer was calibrated using the Raman band at 520 cm^{-1} of a standard SiO_2 sample.

The UV–VIS spectra were recorded using a UV3600 UV–vis spectrophotometer with Shimadzu ISR-3100 integrating sphere attachment having an angle of incident light of 0–8°, two light sources: D2 (deuterium) lamp for the ultraviolet range and WI (halogen) lamp for the visible range and a PMT (photomultiplier tube) detector. The spectra were recorded in the range of 190–800 nm (the switching wavelength of the lamps is between 282 nm and 393 nm) with a wavelength step of 2 nm, having the slit width of 8 nm. The spectra were measured using samples diluted with extra pure barium sulfate (Nacalai Tesque).

The reducibility of the catalysts was studied by temperature programmed reduction under hydrogen (H_2-TPR). Experiments were performed using a CATLAB microreactor – MS system (Hiden Analytical, UK) under a flow of 5% H_2/Ar mixture through the CATLAB's packed micro-reactor containing about 35 mg of sample, which was heated at a constant rate of 20 °C min^{-1} up to 850 °C. The system

Please cite this article in press as: G. Mitran, et al., Propane oxidative dehydrogenation over VO_x/SBA-15 catalysts, Catal. Today (2016), http://dx.doi.org/10.1016/j.cattod.2016.12.014

was maintained for 1 h at 850 °C under H_2/Ar flow to complete the reduction.

2.4. Catalytic tests

The catalytic ODH of propane was carried out in a fixed bed quartz tube down-flow reactor with an internal diameter of 15 mm, as previously described [33]. The catalyst bed (0.1 g) was supported by quartz wool, while the dead volumes before and after the catalyst bed were filled with quartz chips in order to minimize potential homogeneous reactions at higher temperatures [1]. The axial temperature profile was measured using an electronic thermometer placed in a thermowell centered in the catalyst bed. The propane – air mixture (with propane-to-oxygen molar ratios between 1 and 4) was fed into the reactor with a space velocity between 1000 and 2000 ml $(\text{min}\, g_{cat})^{-1}$. Catalytic reactions were performed at atmospheric pressure in the temperature range from 450 to 600 °C.

In a typical reaction run, the reactor was heated to the desired temperature in a reactants' flow, and then allowed to stabilize for 1 h before the first analysis was made. Each run was carried out over a period of 2–3 h, until two consecutive measurements were identical. The reaction products were analyzed with a ThermoQuest Trace Gas Chromatograph equipped with a thermal conductivity detector (TCD) using a CTR I column, and a flame ionization detector (FID) using an alumina column. The presence of oxygenates was checked on a ThermoFinnigan Gas Chromatograph equipped with a flame ionization detector (FID) using a DB-5 column.

The major products observed under our reaction conditions were propene, CO, CO_2 and cracking products (methane and ethylene), with trace amounts of oxygenates (acrolein, acetaldehyde). The latter were not considered for calculating the catalytic performances as the carbon balance based on the major products was in all runs higher than 97%. Conversion of propane and product selectivities were expressed as mol% on a carbon atom basis.

3. Results and discussion

3.1. Catalysts characterization

All the samples showed adsorption-desorption isotherms (Fig. 1) of type IV, typical for mesoporous materials, with H1 hysteresis loops characteristic to well-defined, relatively uniform cylindrical pores, with a narrow size distribution. The amount of adsorbed nitrogen was significantly higher for the SBA-15 support than for the V-containing samples. Regarding the latter samples, it was similar for the lower three V loadings, then decreased for the 10V and 11V samples. The SBA-15 sample has narrow and bimodal pores with maxima at about 5.9 and 7.1 nm, while for the V-containing samples the pore distributions become unimodal, with an average pore diameter of 6.3–6.4 nm (Fig. S1). This suggests that V deposition blocked the low-size pores of the SBA-15 support, in line with the significantly lower surface area of the V-containing samples (Table 1). On the other hand, there were no significant changes of the average pore diameter among the V-containing samples (Table 1) suggesting a well and uniform deposition of vanadium species onto the SBA-15 walls.

The SEM images (Fig. S2) show the surface morphology of the catalyst samples. They all have the same fiber-like morphology of the SBA-15 support, with primary particles coupled along their length and having a width of ca. 5 μm, proving that no morphological changes were produced by V deposition.

The chemical composition, estimated by EDX, and textural properties of the prepared catalysts are presented in Table 1. Both the surface area (793 $m^2\ g^{-1}$) and the pore volume (0.85 $cm^3\ g^{-1}$) of the SBA-15 support were higher than those of the V-containing systems. A decrease in the BET surface areas (from 502 to 419 $m^2\ g^{-1}$) and pore volumes (from 0.82 to 0.69 $cm^3\ g^{-1}$) is observed as the V content increases. Changes in textural parameters upon vanadium impregnation are often reported in the literature, attributed to VO_x species entering the support pores or to a partial destruction of the framework [9,17]. These changes could also be due, at least partly, to the treatment in water of SBA-15 material during the impregnation process, as previously reported by Galarneau et al. [34]. For our samples, it can be concluded that well-organized mesoporous V-containing SBA-15 catalysts with a high surface area were obtained for all V loadings.

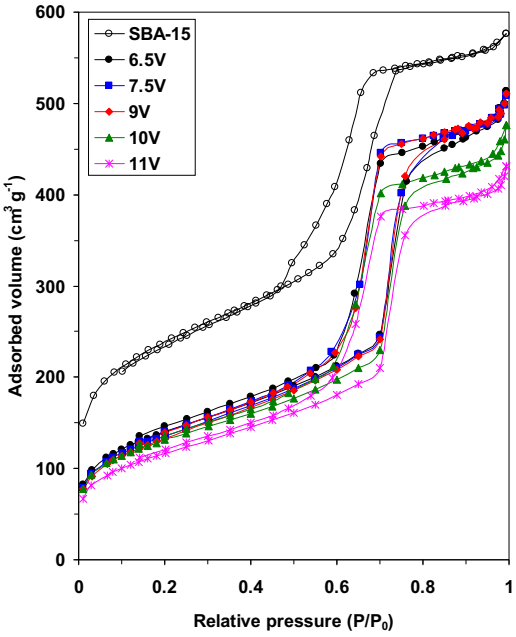

Fig. 1. Nitrogen adsorption-desorption isotherms of bare SBA-15 and VO_x/SBA-15 samples.

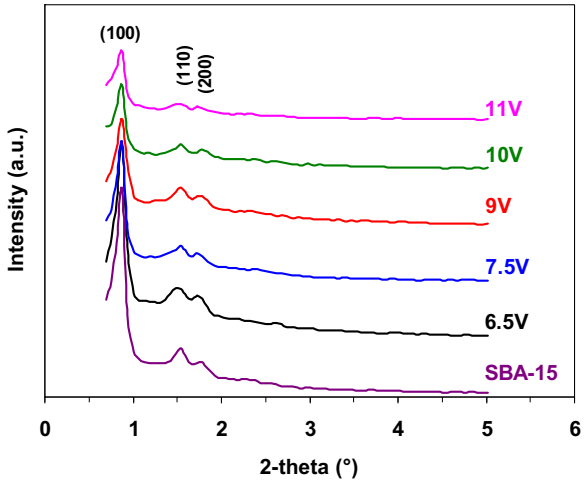

Fig. 2. Small-angle diffractograms of the SBA-15 support and VO_x/SBA-15 catalyst samples.

The VO_x surface density, defined as the number of vanadium atoms per square nanometer of the catalyst, was calculated, the results obtained being tabulated in Table 1. It provides a convenient parameter for comparing catalysts with different surface areas. A more detailed discussion of the results will follow.

Fig. 2 shows the small-angle XRD patterns of the calcined samples, with three resolved peaks at 0.88, 1.54 and 1.75° 2θ, attributed

Please cite this article in press as: G. Mitran, et al., Propane oxidative dehydrogenation over VO_x/SBA-15 catalysts, Catal. Today (2016), http://dx.doi.org/10.1016/j.cattod.2016.12.014

Table 1
The chemical composition and textural properties of the SBA-15 support and VO_x/SBA-15 catalysts.

Sample	V loading (wt%)	BET surface area ($m^2\ g^{-1}$)	Average pore diameter (nm)	Total pore volume ($cm^3\ g^{-1}$)	V density (nm^{-2})
SBA-15	–	793	5.9 and 7.1	0.85	–
6.5V	6.6	502	6.4	0.82	1.6
7.5V	7.4	487	6.4	0.81	1.8
9V	8.9	480	6.3	0.81	2.2
10V	10.2	468	6.4	0.76	2.6
11V	10.9	419	6.3	0.69	3.1

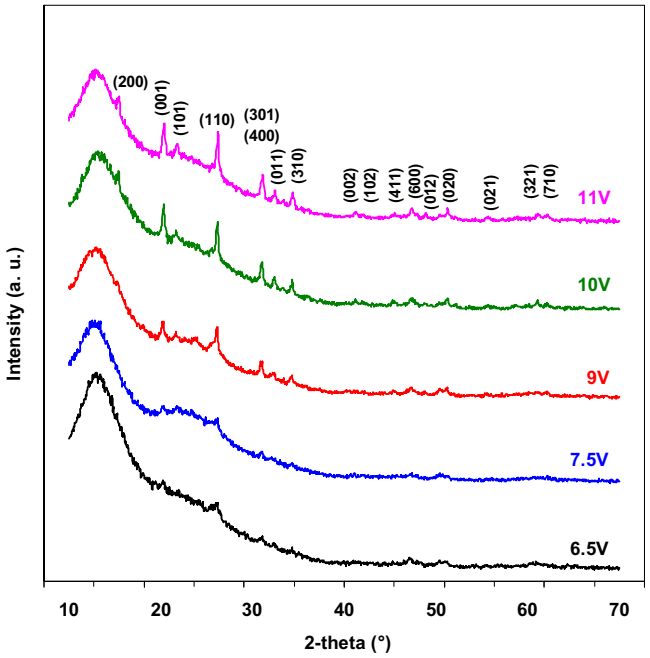

Fig. 3. Wide-angle diffractograms of the calcined VO_x/SBA-15 catalyst samples (V_2O_5 phase indexed).

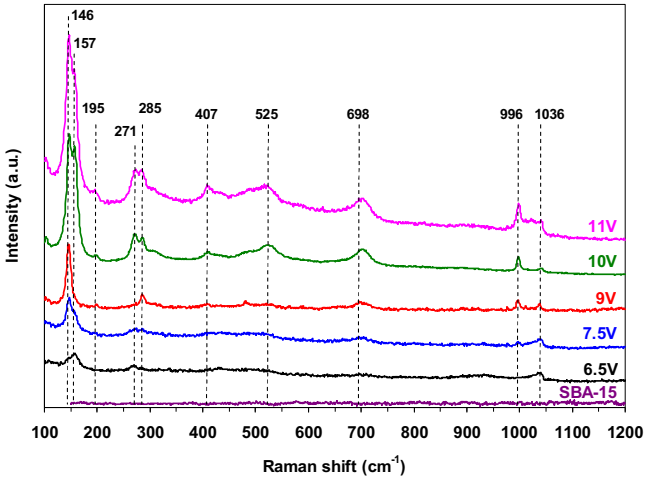

Fig. 4. Raman spectra of bare SBA-15 and VO_x/SBA-15 samples.

to the (100), (110) and (200) reflections, respectively, features of SBA-15 with hexagonal symmetry [24,25]. As the vanadium loading increases, the intensity of the (100) peak weakens. This can be due to the partial blocking of the SBA-15 mesopores and decline of long-range order of hexagonally arranged porosity [24] or, to the deposition of vanadia onto the pore walls, as vanadium has a higher absorption factor for X-rays than silicon [35]. However, all three peaks are visible at all V loadings, showing that the SBA-15 structure is retained upon vanadium impregnation.

Fig. 3 shows the wide-angle diffractograms. It can be observed that all samples have a broad peak centered at ca. 13.5° 2θ, attributed to the amorphous SBA-15 support. The presence of diffraction peaks at higher 2θ angles indicates the presence of V_2O_5 crystallites (PDF 03-65-0131; characteristic peaks at ca. 15.5, 20, 22, 26 and 31° 2θ) [36,37]. The most intense of them (2θ = 20 and 26°) can barely be observed in the 6.5V sample, accounting for the high dispersion of the vanadia species, likely as mono- and polyvanadate species. As the vanadium loading increases, the V_2O_5 peaks become more intense. From the practical point of view, a monolayer surface coverage for the 6.5V sample can be considered, as it is close to the point when vanadia species start to condense to nanocrystalline oxide-like species as shown by XRD results for the samples with higher V content. From the theoretical point of view, the monolayer (a bidimensional surface vanadium oxide overlayer on the support [14]) was defined as the need for 4.98×10^{14} V_2O_5 species nm^{-2} to completely cover the surface of the support [38], or as 0.10 wt% V_2O_5 per m^2 of surface [39]. Monolayer surface coverage of the surface vanadia on oxide supports has been estimated from structural and experimental determinations. From the V—O bond lengths of crystalline V_2O_5, monolayer coverage is estimated at 10 VO_x nm^{-2} for a bidimensional polyvanadate layer and at 2.5 VO_x nm^{-2} for isolated monomeric vanadia units. Monolayer surface coverage determined from Raman spectroscopy was found to be ca. 7–8 VO_x nm^{-2} for different oxide supports (Al_2O_3, TiO_2, ZrO_2, Nb_2O_5 and CeO_2) with the exception of silica-supported vanadia, which exhibited a maximum surface coverage of only 0.7 VO_x nm^{-2} [40 and References therein]. Other studies found 1.1 VO_x nm^{-2} for monolayer coverage on silica [5,9], attributed to the weak interaction between the vanadium oxide and the support, leading to a poor dispersion of the precursor salt [5,14]. This is an expected result, as both V_2O_5 and SBA-15 have an acidic character. It has been reported that the dispersion of the vanadium oxide as well as its structure can be understood on the basis of the different acid-base character of the different supports. The acidity of the metal oxide is related to the pH at which the surface possesses zero surface charge (point of zero charge, PZC, or isoelectric point, IE). IE of V_2O_5 was measured as 1.4 [38], while for SBA-15 it was 4.2 [41]. A weaker interaction of the vanadium oxide with another acidic oxide, SBA-15 here, will favour the agglomeration of the VO_x units to form V_2O_5.

In this study a monolayer coverage on SBA-15 can be approximated to be 1.6 VO_x nm^{-2}. To the best of our knowledge, this is the highest monolayer coverage of vanadia on SBA-15 reported so far. The reason for this higher coverage can be explained by the fact that the support was re-hydrated before impregnation, which led to a better dispersion of the surface species.

Raman spectroscopy has a higher sensitivity to the presence of oxide-like species than XRD [9]. The Raman spectrum of the SBA-15, presented in Fig. 4, exhibits no characteristic bands, while those of the V-containing samples show bands corresponding to different vanadium species present on the surface. Thus, the 6.5V catalyst shows bands at ca. 1036 cm^{-1} attributed to the symmetric stretch-

Please cite this article in press as: G. Mitran, et al., Propane oxidative dehydrogenation over VO_x/SBA-15 catalysts, Catal. Today (2016), http://dx.doi.org/10.1016/j.cattod.2016.12.014

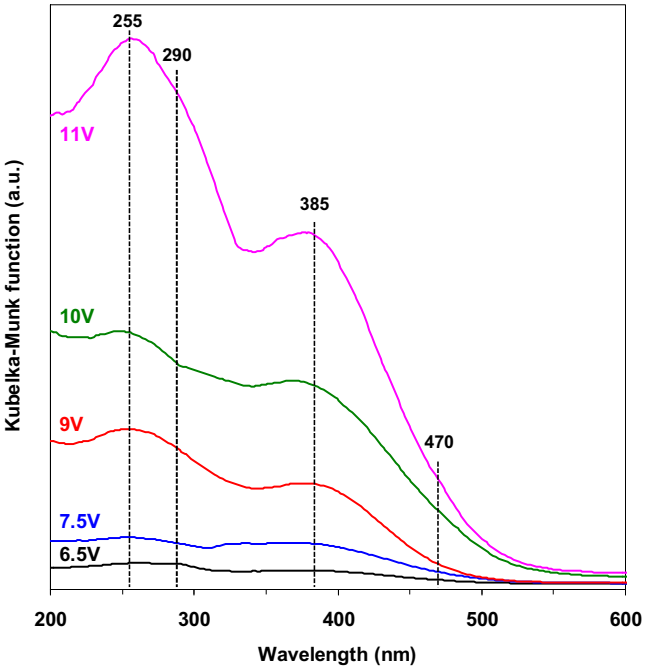

Fig. 5. UV–vis DRS spectra of the VO_x/SBA-15 samples.

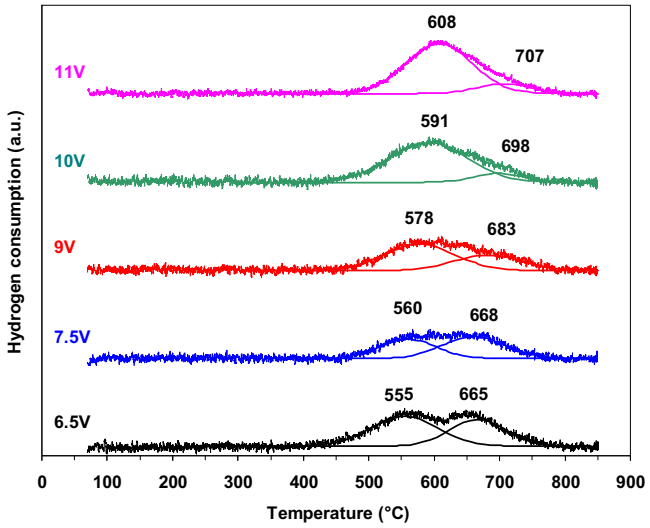

Fig. 6. H_2-TPR profiles for the VO_x/SBA-15 samples.

ing mode of the vanadyl bond (V=O) in isolated monomeric VO_4^{3-} species [14,20,27], and at 157 and 271 cm^{-1}, assigned to hydrated amorphous polymeric species on the surface [27]. As the vanadium loading increases, the intensity of the 1036 cm^{-1} band diminishes, while those belonging to polymeric species intensify. New bands at 996, 698, 525, 407, 285, 195, and 146 cm^{-1}, assigned to V_2O_5 crystallites on the support [6,27,42], appear and increase in intensity, in line with the XRD results. Since the ratio of scattering cross section of crystalline V_2O_5 relative to isolated monovanadate and polyvanadate species was estimated to be very large (approximately 10 [6,17,20]), V_2O_5 nanoparticles may exist in low amounts in the 7.5V and 9V samples.

UV–vis DRS spectra give additional structural information on the surface VO_x species, the energy of the oxygen-vanadium charge transfer bands indicating the coordination of the V^{5+} center [20]. The SBA-15 support exhibited only a very low intensity spectrum (not shown). For the VO_x/SBA-15 catalyst samples (Fig. 5), the spectra show an absorption band at ca. 255 nm with a shoulder at ca. 290 nm and another one at ca. 385 nm, with intensities increasing with vanadium loading. The first band can be attributed to low-energy charge transfer transitions between O^{2-} ligands and V^{5+} species in isolated tetrahedral VO_4^{3-} structures on the SBA-15 surface [11,18,20,43], while the shoulder arises from the charge transfer transitions in oligomeric $(VO_4^{3-})_n$ structures [43]. The second band can be assigned to 2D polymeric structures of pentacoordinated vanadium ions, i.e. polyvanadates [43]. Only in the 10V and 11V samples a shoulder was observed at around 470 nm, indicating the presence of "bulk-like" vanadia crystallites [20,43]. These findings are in line with the XRD and Raman results and confirm the presence of mono- and oligomeric $(VO_4^{3-})_n$ species and of polyvanadate structures on the surface of all samples, and of bulk-like crystallites at high vanadium loading.

The selectivity for oxidative dehydrogenation products depends on the reactivity and availability of the surface oxygen species: when surface intermediates have a high probability to react with lattice oxygen species, a lower selectivity to propene is obtained [1]. Therefore, hydrogen temperature-programmed reduction (TPR) profiles were recorded to obtain information on the reducibility of the catalyst samples. For all the catalysts, reduction occurred in the range 500–700 °C (Fig. 6), the obtained TPR profiles being deconvoluted into two main features. The 6.5V sample shows two broad equal area peaks centered at 555 and 665 °C, respectively. The first peak can be attributed to the reduction of monomeric and oligomeric $(VO_4^{3-})_n$ species in tetrahedral coordination geometry [43], while the second one can be assigned to the reduction of V_2O_5 clusters [43]. The presence of V_2O_5 clusters at low V loadings is not unexpected as it has already been evidenced for silica-supported V_2O_5 catalysts [43 and References therein]. As the V loading increases both reduction maxima shift to higher temperatures, while the peaks remain broad. Thus, for the first reduction peak the temperature of the maximum H_2 consumption increases continuously from 555 °C for 6.5V sample to 608 °C for 11V sample, while for the second reduction peak it increases from 665 to 707 °C. On the other hand, the intensity of the first reduction peak increases while that of the second one continuously decreases. A perusal of these data by analogy with previous results on the reducibility of silica-supported V_2O_5 catalysts [20,43 and References therein] clearly suggests that besides the tetrahedral mono- and oligomeric $(VO_4^{3-})_n$ species mainly identified in the 6.5V sample, less reducible square-pyramidal polymeric structures, *i.e.* polyvanadates, become predominant with increasing the V loading. At the same time, the V_2O_5 clusters responsible for the second reduction peak of the 6.5V sample evolve toward less reducible V_2O_5 crystallites at high V loadings. This interpretation is in line with the XRD, Raman and UV–vis data of the samples.

It is noteworthy that, except for H_2-TPR, all the characterization results discussed above were obtained at room temperature. However, it has been shown that for silica supported catalysts in reaction conditions and in the presence of water (reaction product), the observed species are not the same as at room temperature [44]. Thus, Launay et al. showed that the molecular structure of VO_x species supported on mesoporous silica strongly depends on the degree of hydration. Dehydration by heating at 400 °C caused depolymerization of the vanadium species leading to increased dispersion and anchoring on the silica support. This dynamic change was completely reversible at rehydration. Therefore, it is highly possible that in the reaction conditions the ratio between monomeric and polymeric species changes to favor the former, the selective species in the ODH process.

Please cite this article in press as: G. Mitran, et al., Propane oxidative dehydrogenation over VO_x/SBA-15 catalysts, Catal. Today (2016), http://dx.doi.org/10.1016/j.cattod.2016.12.014

Table 2
Propane conversion and product selectivity values in the ODH of propane. Propane-to-oxygen mol ratio = 2:1, space velocity = 1500 ml $(g_{cat}\ min)^{-1}$.

Catalyst sample	Temperature (°C)	Propane conversion (%)	Selectivities (%)			E_{act}[a] (kJ mol^{-1})
			Propene	Cracking	CO_x	
6.5V	450	0.5	87	1	12	158
	500	2.8	80	2	18	
	550	12.1	68	3	29	
	600	16.3	66	5	29	
7.5V	450	0.6	84	1	15	152
	500	3.9	74	1	25	
	550	12.9	64	2	34	
	600	17.5	62	3	35	
9V	450	0.8	83	1	16	141
	500	5.1	72	2	26	
	550	13.7	59	5	36	
	600	18.5	57	7	36	
10V	450	1.1	73	1	26	130
	500	6.0	65	1	34	
	550	14.9	44	2	54	
	600	19.6	41	5	54	
11V	450	1.5	71	1	28	119
	500	6.8	58	1	41	
	550	16.3	39	2	59	
	600	21.6	38	4	58	

[a] Apparent activation energy.

3.2. Catalytic study

No significant reaction took place in the absence of catalysts [45]. For all the VO_x/SBA-15 samples, the main products were propene and carbon oxides, with minor amounts of cracking products (methane and ethylene) and trace amounts of oxygenates. Oxygen was never completely consumed, therefore the catalytic activity and selectivity to products were not influenced by a lack of reactant.

The catalytic activities strongly depend on the temperature and vanadium content. As it can be seen in Table 2, conversion values increase with both temperature and V loading, reaching ca. 22% for the 11V sample at 600 °C. At the same time propene selectivity decreased mainly for the benefit of carbon oxides. The highest propene selectivities on the entire temperature range were obtained for the 6.5V catalyst, with values decreasing for higher V content. Correlating these findings with the characterization data, we conclude that the active species for ODH reaction are the isolated vanadium species on the surface, while the vanadia crystallites formed at higher loadings lead mainly to carbon oxides. Indeed, the isolated active sites favor propene formation and preclude its further oxidation to CO_x, while in V_2O_5 crystallites this site isolation is no longer possible and, therefore, subsequent complete oxidation becomes preponderent [18,24].

Notably, these catalytic performances are comparable with [9,19] or better than [8] those already published for similar VO_x/SBA-15 catalysts, especially concerning propene selectivity. This is obviously due to the presence of significant amounts of mono- and oligomeric $(VO_4^{3-})_n$ species even at high vanadium loadings, as suggested by UV–vis spectroscopy. Higher propane conversions reported in other studies [18,22,29] were obtained in significantly different reaction conditions, i.e. much lower GHSV.

The apparent activation energies (E_{act}) corresponding to the propane transformation on the VO_x/SBA-15 catalysts have been calculated (Table 2) from the Arrhenius plots presented in Fig. S3. They decreased with increasing V content, in line with the observed increase of the catalytic activity. This suggests that the nature of the catalytic site changes with increasing V content, as tetrahedral VO_x species transform into square-pyramidal polymeric ones and then into V_2O_5 crystallites, in line with the characterization data. Thus, based on the characterization results and the data in Table 2, tetrahedral mono- and oligomeric $(VO_4^{3-})_n$ species are less active (lower propane conversion, higher activation energies) but highly selective (higher selectivity to propene), while square-pyramidal polymeric species and even more V_2O_5 crystallites are more active (higher propane conversion, lower activation energies) but less selective in ODH reaction of propane.

It is noteworthy that the apparent activation energies values listed in Table 2 are in line with literature data for silica-supported V catalysts, ranging from 80 to 160 kJ mol^{-1} for similar V density on the surface [14].

The effect of the conversion on the selectivities has been studied for 6.5V, 9V and 10V catalysts at 550 °C and a propane-to-oxygen molar ratio equal to 2, by varying the space velocity in the range 1000–2000 ml $(g_{cat}\ min)^{-1}$. As expected, the selectivity to propene decreased in all cases with increasing conversion (Fig. 7). The extrapolation to zero conversion results in 100% selectivity to propene and zero selectivity for CO_x, showing that propene is the only primary product on SBA-15-supported V catalysts irrespective to the V content, as was proved for other V-based catalysts [1,14]. This clearly suggests that the process takes place in successive steps, the first one being the oxidative dehydrogenation of propane into propene, which is then oxidized to carbon oxides, while the direct combustion of propane does not occur in measurable amounts on the studied catalysts. The same conclusion was also reached by other studies of propane ODH on supported vanadia catalysts [14,30].

The influence of the propane-to-oxygen molar ratio on the catalytic performances was also investigated for the 9V catalyst. The reactions were performed at 550 °C and the space velocity fixed at 1500 ml $(g_{cat}\ min)^{-1}$, while modifying the propane-to-oxygen ratios between 1 and 4. The propane conversion strongly decreased when the propane-to-oxygen molar ratio increased from 1 to 4 (Fig. 8), while the selectivity to propene increased at the expense of carbon oxides. These results could be explained by the decrease of the available oxygen related to the increase in the propane-to-oxygen ratio.

4. Conclusion

VO_x/SBA-15 catalysts with different vanadia loadings were prepared by a modified wet impregnation method, characterized and

Please cite this article in press as: G. Mitran, et al., Propane oxidative dehydrogenation over VO_x/SBA-15 catalysts, Catal. Today (2016), http://dx.doi.org/10.1016/j.cattod.2016.12.014

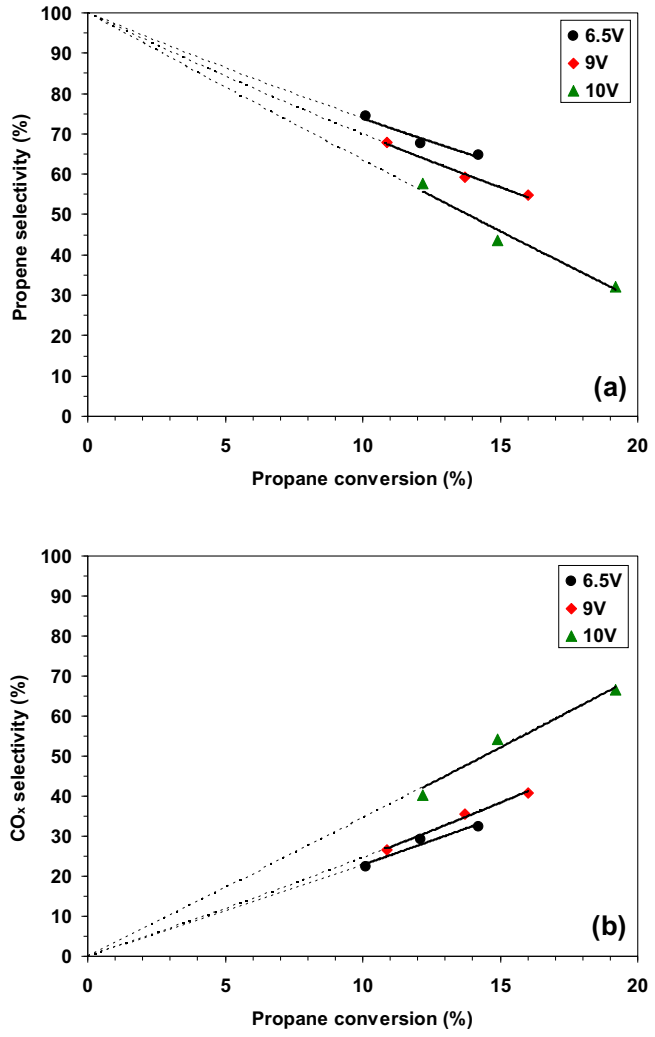

Fig. 7. Effect of propane conversion on the propene selectivity (a) and CO_x selectivity (b) in the propane ODH over VO_x/SBA-15 catalysts. Reaction temperature of 550 °C, propane-to-oxygen molar ratio of 2 and space velocity varied from 1000 to 2000 ml $(g_{cat}\ min)^{-1}$.

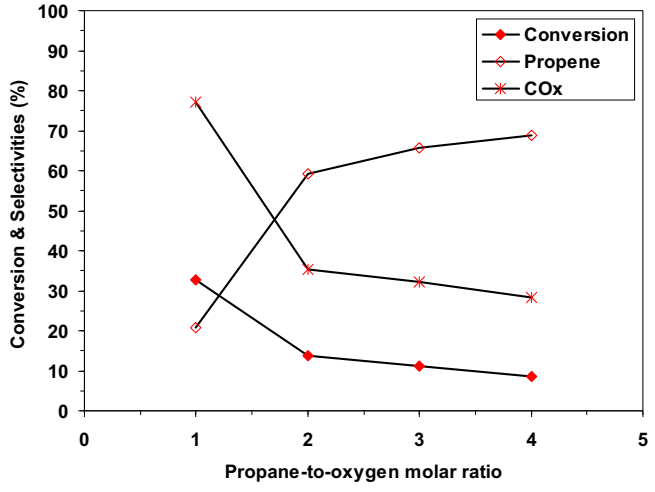

Fig. 8. Effect of propane-to-oxygen molar ratio on the oxidative dehydrogenation of propane over the 9V catalyst. Reaction temperature of 550 °C, space velocity of 1500 ml $(g_{cat}\ min)^{-1}$.

their reactivity studied in the propane ODH. A monolayer coverage vanadium density of 1.6 $VO_x\ nm^{-2}$ was obtained for the sample containing 6.6 wt% V on SBA-15 (6.5V catalyst), the highest reported so far on this support. At low vanadium content tetrahedral mono- and oligomeric $(VO_4^{3-})_n$ species are predominant on the catalyst surface where they coexist with vanadia clusters. As vanadium content increases, square-pyramidal polyvanadate species become predominant and coexist with V_2O_5 crystallites, with higher activity but lower selectivity to propene. Propane conversion increases with both temperature and V content, with concomitant decreasing of propene selectivity mainly to the benefit of CO_x. Increasing the propane-to-oxygen molar ratio from 1 to 4, the propane conversion decreased from 33 to 9%, but the propene selectivity increased from 20 to 69% for the 9V catalyst. Conversion-selectivity plots show that propene is the only primary product at all V loadings. The catalytic performance of the studied catalysts is comparable with or even better than other similar VO_x/SBA-15 catalysts, especially concerning propene selectivity. This feature is related to the presence of significant amounts of mono- and oligomeric $(VO_4^{3-})_n$ species even at high vanadium loadings.

Aknowledgements

This research did not receive any specific grant from funding agencies in the public, commercial, or not-for-profit sectors.

Appendix A. Supplementary data

Supplementary data associated with this article can be found, in the online version, at http://dx.doi.org/10.1016/j.cattod.2016.12.014.

References

[1] H.K. Kung, Adv. Catal. 40 (1994) 1–38.
[2] R. Grabowski, Catal. Rev. 48 (2006) 199–268.
[3] Z. Nawaz, Rev. Chem. Eng. 31 (2015) 413–436.
[4] W. Daniell, A. Ponchel, S. Kuba, F. Andrele, T. Weingand, D.H. Gregory, H. Knözinger, Top. Catal. 30 (2002) 65–74.
[5] J. Santamaria-Gonzales, J. Luque-Zambrana, J. Merida-Robles, P. Maireles-Torres, E. Rodriguez-Castellon, A. Jimenez-Lopez, Catal. Lett. 68 (2000) 67–73.
[6] H. Dai, A.T. Bell, E. Iglesia, J. Catal. 221 (2004) 491–499.
[7] J.M. Lopez Nieto, Top. Catal. 41 (2006) 3–15.
[8] P. Gruene, T. Wolfram, K. Pelzer, R. Schlögl, A. Trunschke, Catal. Today 157 (2010) 137–142.
[9] R. Bulánek, P. Čičmanec, H. Sheng-Yang, P. Knotek, L. Čapek, M. Setnička, Appl. Catal. A: Gen. 415–416 (2012) 29–39.
[10] E.V. Kondratenko, M. Cherian, M. Baerns, D. Su, R. Schlögl, X. Wang, I.E. Wachs, J. Catal. 234 (2005) 131–142.
[11] P. Kuśtrowski, Y. Segura, L. Chmielarz, J. Surman, R. Dziembaj, P. Cool, E.F. Vansant, Catal. Today 114 (2006) 307–313.
[12] R.B. Watson, U.S. Ozkan, J. Catal. 191 (2000) 12–29.
[13] H. Arakawa, M. Aresta, J.N. Armor, M.A. Barteau, E.J. Beckman, A.T. Bell, J.E. Berkaw, C. Creutz, E. Dinjus, D.A. Dixon, K. Domen, D.L. DuBois, J. Eckert, E. Fujita, D.H. Gibson, W.A. Goddard, D.W. Goodman, J. Keller, G.J. Kubas, H.H. Kung, J.E. Lyons, L.E. Manzer, T.J. Marks, K. Morokuma, K.M. Nicholas, R. Periana, L. Que, J. Rostrup-Nielson, W.M.H. Sachtler, L.D. Schmidt, A. Sen, G.A. Somorjai, P.C. Stair, B.R. Stults, W. Tumas, Chem. Rev. 101 (2001) 953–996.
[14] C.A. Carrero, R. Schloegl, I.E. Wachs, R. Schomaecker, ACS Catal. 4 (2014) 3357–3380.
[15] J.C. Védrine, I. Fechete, C. R. Chim. 19 (2016) 1203–1225.
[16] A. Corma, J.M. Lopez Nieto, N. Paredes, M. Perez, Y. Shen, H. Gao, S.L. Suib, Stud. Surf. Sci. Catal. 72 (1992) 213–220.
[17] S.A. Karakoulia, K.S. Triantafyllidis, G. Tsilomelekis, S. Boghosian, A.A. Lemonidou, Catal. Today 141 (2009) 245–253.
[18] M. Piumetti, B. Bonelli, P. Massiani, S. Dzwigaj, I. Rossetti, S. Casale, M. Armandi, C. Thomas, E. Garrone, Catal. Today 179 (2012) 140–148.
[19] R. Bulánek, A. Kalužová, M. Setnička, A. Zukal, P. Čičmanec, J. Mayerová, Catal. Today 179 (2012) 149–158.
[20] Y.-M. Liu, W.-L. Feng, T.-C. Li, H.-Y. He, W.-L. Dai, W. Huang, Y. Cao, K.-N. Fan, J. Catal. 239 (2006) 125–136.
[21] J. Xu, M. Chen, Y.-M. Liu, Y. Cao, H.-Y. He, K.-N. Fan, Microporous Mesoporous Mater. 118 (2009) 354–360.
[22] Y.-M. Liu, Y. Cao, S.-R. Yan, W.-L. Dai, K.-N. Fan, Catal. Lett. 88 (2003) 61–67.

[23] C. Hess, I.J. Drake, J.D. Hoefelmeyer, T.D. Tilley, A.T. Bell, Catal. Lett. 105 (2005) 1–8.
[24] W. Liu, S.Y. Lai, H. Dai, S. Wang, H. Sun, C.T. Au, Catal. Lett. 113 (2007) 147–154.
[25] G. Wang, L. Zhang, J. Deng, H. Dai, H. He, C.T. Au, Appl. Catal. A: Gen. 355 (2009) 192–201.
[26] M.A. Bañares, X. Gao, J.L.G. Fierro, I.E. Wachs, Stud. Surf. Sci. Catal. 110 (1997) 295–304.
[27] G. Du, S. Lim, M. Pinault, C. Wang, F. Fang, L. Pfefferle, G.L. Haller, J. Catal. 253 (2008) 74–90.
[28] W. Liu, S.Y. Lai, H. Dai, S. Wang, H. Sun, C.T. Au, Catal. Today 131 (2008) 450–456.
[29] F. Ying, J. Li, C. Huang, W. Weng, H. Wan, Catal. Lett. 115 (2007) 137–142.
[30] C. Hess, U. Wild, R. Schlögl, Microporous Mesoporous Mater. 95 (2006) 339–349.
[31] A. Dinse, S. Khennache, B. Frank, C. Hess, R. Herbert, S. Wrabetz, R. Schlögl, R. Schomäcker, J. Mol. Catal. A: Chem. 307 (2009) 43–50.
[32] D. Zhao, Q. Huo, J. Feng, B.F. Chmeka, G.D. Stucky, J. Am. Chem. Soc. 120 (1998) 6024–6036.
[33] G. Mitran, T. Cacciaguerra, S. Loridant, D. Tichit, I.-C. Marcu, Appl. Catal. A: Gen. 417–418 (2012) 153–162.
[34] A. Galarneau, M. Nader, F. Guenneau, F. Di Renzo, A. Gedeon, J. Phys. Chem. C 111 (2007) 8268–8277.
[35] L. Vradman, M.V. Landau, M. Herskowitz, V. Ezersky, M. Talianker, S. Nikitenko, Y. Koltypin, A. Gedanken, J. Catal. 213 (2003) 163–175.
[36] O. Schwarz, B. Frank, C. Hess, R. Schomäcker, Catal. Commun. 9 (2008) 229–233.
[37] V.N. Shevchuk, Y.N. Usatenko, P.Y. Demchenko, O.T. Antonyak, R.Y. Serkiz, Chem. Metals Alloys 4 (2011) 67–71.
[38] T. Blasco, J.M. Lopez Nieto, Appl. Catal. 157 (1997) 117–142.
[39] G.C. Bond, J. Perez Zurita, S. Flamerz, P.J. Gellings, H. Bosh, J.G. Van Ommen, B.J. Kip, Appl. Catal. 22 (1986) 361–378.
[40] I.E. Wachs, B.M. Weckhuysen, Appl. Catal. A: Gen. 157 (1997) 67–90.
[41] M. Kosmulski, J. Colloid Interface Sci. 337 (2009) 439–448.
[42] M.V. Bosco, M.A. Bañares, M.V. Martínez-Huerta, A.L. Bonivardi, S.E. Collins, J. Mol. Catal. A: Chem. 408 (2015) 75–84.
[43] F. Arena, F. Frusteri, G. Martra, S. Coluccia, A. Parmaliana, J. Chem. Soc. Faraday Trans. 93 (1997) 3849–3854.
[44] H. Launay, S. Loridant, A. Pigamo, J.L. Dubois, J.M.M. Millet, J. Catal. 246 (2007) 390–398.
[45] G. Mitran, A. Urda, N. Tanchoux, F. Fajula, I.-C. Marcu, Catal. Lett. 131 (2009) 250–257.

Please cite this article in press as: G. Mitran, et al., Propane oxidative dehydrogenation over VO_x/SBA-15 catalysts, Catal. Today (2016), http://dx.doi.org/10.1016/j.cattod.2016.12.014